Supporting Information for:

Behaviour of aluminium, arsenic and vanadium during the neutralisation of red mud leachate by HCl, gypsum, or seawater

Ian T. Burke[1*], Caroline L. Peacock[1], Cindy L. Lockwood[1], Douglas I. Stewart[2], Robert J G Mortimer[1], Michael Ward[3], Philip Renforth[4], Katalin Gruiz[5] and William M. Mayes[6]

[1] Earth Surface Science Institute, School of Earth and Environment, University of Leeds, Leeds LS2 9JT, UK. [*]Corresponding Author's E-mail: i.t.burke@see.leeds.ac.uk; Phone: +44 113 3437532; Fax: +44 113 3435259

[2] School of Civil Engineering, University of Leeds, Leeds LS2 9JT, UK.

[3] School of Process, Environmental and Materials Engineering, University of Leeds, Leeds LS2 9JT, UK.

[4] Department of Earth Sciences, University of Oxford, South Parks Road, Oxford, OX3 0DP, UK

5 Department of Applied Biotechnology and Food Science, Budapest University of Technology and Economics. 1111 Budapest, St. Gellért sq. 4. Hungary.

[6] Centre for Environmental and Marine Sciences, University of Hull, Scarborough, YO11 3AZ, UK.

In preparation for *Environmental Science and Technology*, 08 May 2013

This section consists of 14 pages, 3 tables and 5 figures.

Section S1. XAS analysis.

Approximately 100 mg of each precipitate was prepared for analysis as moist pastes in Perspex holders with Kapton windows. The dried sediment sample (M7b) was prepared for XAS analysis by vigorous homogenisation in an acid washed agate mortar and pestle and pressed into 8 mm pellets held in Kapton™ tape. Standard materials were also prepared as pressed pellets using cellulose as a diluent to reduce chemical thickness (to achieve an edge step between 0.5 and 1.5 in transmission mode, see below) and held in Kapton™ tape. Solutions of sodium arsenate and sodium arsenite were prepared at 1000 mg L^{-1} and held in polythene bags for analysis. A sodium vanadate solution was prepared in 0.1 mol.L^{-1} NaOH, also at 1000 mg.L^{-1}, and held in polythene bags as above. Vanadate adsorbed to $Al(OH)_3$ was prepared by suspension of 1 g $Al(OH)_3$ in 1 L DIW and adding 1 ml of 1000 mg L^{-1} $NaVO_4$ (made up in 0.01 mol L^{-1} NaOH at pH 12). The mixed suspension was stirred for 48 hours and the final pH was 7.0. The V-$Al(OH)_3$ solid was recovered by centrifugation (2000 *g*; 10 mins) and prepared for analysis as a moist paste as above. A hydrous Ca-arsenate phase was precipitated by reaction of 10 ml of 0.1 mol L^{-1} $NaHAsO_4$ solution with 20 ml of 0.5 mol L^{-1} $CaCl_2$ solution at pH 7. The resultant precipitate was separated by centrifugation (2000 *g*; 10 mins), washed twice in 1.0 mol L^{-1} $CaCl_2$ solution and dried at 40 ^{o}C prior to being diluted with cellulose (1:10). The diluted powder was prepared as a pressed pellet for XAS analysis.

XAS spectra were collected at the As and V K-edges (11867 and 5465 eV respectively) on beamline I18 at the Diamond Light Source operating at 3 GeV with a typical current of 200 mA, using a nitrogen cooled Si(111) double crystal monochromator and focussing optics. A pair of plane mirrors was used to reduce the harmonic content of the beam and Kirkpatrick-Baez mirrors were used to produce a relatively unfocused beam (approximately 0.5mm diameter at the sample). For standards prepared as pressed pellets, K-edge spectra were collected in transmission mode at room temperature (~295 °K). For samples and solutions, data were collected in fluorescence mode using a 9 element solid state Ge detector at room temperature. As K-edge spectra were found to be strongly affected by beam damage presenting as an apparent change in As speciation that increased in magnitude with increased exposure to the beam. To mitigate this effect, only single As K-edge EXAFS spectra were collected (~25mins) from a spot within the sample and the sample stage automatically moved to expose an unaffected part of the sample before subsequent scans.

Multiple scans were averaged to improve the signal to noise ratio using Athena version 0.8.061 [1]. For XANES spectra absorption was also normalised in Athena over the full data range and plotted from approximately -15 eV to +30 eV relative to the edge position with no correction required for drift in E_0. V data was calibrated using E_0 measured from thin metal foil, and As data was calibrated using the white line position measured from the sodium arsenate standard. The V pre-edge peak energy was determined by calculation of the area normalised centroid energy position following the method of Chaurand et al. [2].

Section S2 As K-edge EXAFS Analysis.

EXAFS data was background subtracted using PySpline v1.1 [3]and analysed in DLexcurv v1.0 [4]using full curved wave theory [5]. Phaseshifts were derived from *ab initio* calculations using Hedin-Lundqvist potentials and von-Barth ground states [6]. Multiple scattering was allowed for as coded in DLexcurv [4, 6]. Multiple scattering calculations require specification of the full three dimensional structure of the As coordination environment (i.e., bond angles in addition to bond lengths). This was done using hypothetical model clusters with C_1 symmetry (SI Figure S1). The spectra for each sample were then fit by refining each model cluster, and the best fit evaluated using the EXAFS R-factor [7], the EXAFS Fit Index (as coded in Binsted et al., [8]) and the reduced Chi^2 values (as coded in EXCURV98 (Binsted, [6] and references therein)). Specifically, reduced Chi^2 values were used to evaluate the fits of each experimental spectrum to various single shell (involving only nearest neighbour oxygens) vs. multiple shell (involving nearest neighbour oxygens and next-nearest neighbour atoms) model clusters. In this way the statistical significance of invoking 2^{nd} shell backscatters was determined. Next-nearest neighbour backscatter shells were only included if the reduced Chi^2 was improved by $\geq$ 10%, compared to a single shell (oxygens only) cluster [9]. It should be noted that, in DLexcurv, the absolute value of reduced Chi^2 is not accurate (as DLexcurv does not require actual experimental statistical errors). Rather, reduced Chi^2 is used as a relative guide where a reduction or minimum indicates an improved fit. Fitting involved the refinement of an energy correction Ef (the Fermi Energy; which for final fits typically varied between ~ -13.3 and -13.7), and the absorber-scatterer distance and the Debye-Waller factor for each shell. The amplitude factor (or AFAC in DLexcurv V1.0) was retained as the default of 1 throughout. During fitting the number of independent data points was always greater than the number of fitted parameters (in DLexcurv

these are N_{ind} and N_{pars}, respectively). N_{ind} was determined using Stern's rule [10] as $2\Delta k\Delta R/\pi + 2$ [11] where Δk and ΔR are the range in *k*- and *R*-space actually fitted. All spectra were fit in *k*-space and no Fourier filtering was performed.

Fourier transforms of the EXAFS spectra were used to obtain an approximate radial distribution function around the central As atom (the absorber atom); the peaks of the Fourier transform can be related to "shells" of surrounding backscattering ions characterised by atom type, number of atoms, absorber-scatterer distance, and the Debye-Waller factor (± 25%), $2\sigma^2$. Atomic distances calculated by DLexcurv have an error of approximately ± 0.02 and ± 0.05 Å in the first and outer shells respectively [12]. Debye-Waller factors are typically 0.002 – 0.02 $2\sigma^2$ for the first shell and 0.02 – 0.04 $2\sigma^2$ for the outer shells [6].

Section S3. Detailed discussion of V-XANES pre-edge peak data.

Charaund et al. [2] proposed an elegant system for interpreting V K-edge XANES spectra based on the detail observation of pre-edge peak intensity and energy position. In this system, data is described in terms of variation in both co-ordination symmetry and valance state. When such a scheme is applied to the data from the HCl precipitate (SI Figure S4) the sample spectrum plots between the V^{4+} and V^{5+} standards. The data might therefore be interpreted as a mixture of several V-phases. However, when data from vanadate adsorbed to oxide and hydroxide surfaces is also considered [13-15], including the vanadate-$Al(OH)_3$ standard from this study, it is clear that lower pre-edge peak intensities are common for adsorbed vanadate.

The very intense vanadate pre-edge peak observed in V^{5+} K-edge spectra at ~5470 eV is due electron transitions from the 1s to overlapping 3d/4p orbitals that are enhanced by the tetrahedral symmetry present [2, 16]. EXAFS analysis of vanadate in sorption co-ordination environments has found that the vanadate tetrahedron becomes distorted [14, 15] and this change of molecular symmetry decreases 1s$\rightarrow$3d/4p transitions producing a less intense pre-edge peak [14, 15]. A similar molecular distortion (and reduced pre-edge peak intensity) is noted for vanadate in polyvanadate species such as sodium metavanadate ($NaVO_3$) [14]. Therefore, detailed analysis of the V K-edge XANES data for the HCl neutralised samples are consistent with vanadate adsorption to neoformed precipitates during neutralisation.

Interestingly, when V K-edge XANES spectra from red mud samples from the Ajka repository are also considered [17], the data plots within the same region as the sorption samples (SI Figure S4). This might due to the presence of several different V valences, but under the Bayer reaction conditions (high OH^-, temperatures and pressures) lower valence forms of V are expected to be rapidly oxidised [18-20]. Therefore, this V K-edge XANES data could also potentially be interpreted as vanadate present in adsorption complexes or as metavanadate phases.

SI Section S4 Detailed discussion of water balance at the Ajka site.

Based on hydrometric data for the Ajka region, annual average rainfall is around 700 mm per year with annual evapo-transpiration in the region of 560mm per year [21]. This evapo-transpiration rate is likely to underestimate water loss in a settlement lagoon with continuous supply of surface water. With a surface area of 0.27 km^2 in the active settlement cell (Cell 10), the water balance would yield a leachate volume of 38000 m^3 $year^{-1}$ (~1.2 L s^{-1}). This assumes that there is no ingress of groundwater into a lined BRDA and no decant of uncontaminated surface drainage in drier areas of the settlement lagoon. Gypsum treatment at a rate of 30g per litre of leachate would require an annual dosage of 1142 tonnes per year.

Table S1. Indicative cost calculations for neutralisation treatment of red mud using HCl, gypsum or seawater addition.

Neutralising Material	Unit Cost	Quantity required (d)	Potential cost (US$ t-1)
Hydrochloric acid	[a]€75-130 t^{-1} (at 33%) [b]US¢ 1.3 – 2.3 mol^{-1}	10 kmol t^{-1}	130-230
Sulphuric acid	[c]€50-120 t^{-1} (at 98%) [b]US¢ 0.7-1.6 mol-1	5 kmol t-1	35-80
Gypsum	[d]£32 t^{-1} [b]US¢ 0.8 mol^{-1}	[e]5 kmol t^{-1}	40
Seawater	negligible for sites adjacent to the coast	*192 t(seawater) t^{-1}	-

a) www.icispricing.com – accessed 26/02/2013

b) US$ 1.5 = GB£ 1, US$ 1.3 = 1 €

c) c) fw.crugroup.com (Sulphuric acid price) - accessed 06/05/2013

d) BGS Minerals Yearbook 2011 – based on import mass:value

e) Based on an acid neutralising capacity of 10 mol kg-1 [22]

*2mol OH mol-1 gypsum, 1.3mol OH mol-1 Mg (40mmol Mg l-1 seawater)

Table S2. Hydrochemical composition of the red mud leachate and treated red mud leachates used for mineral saturation modelling

Determinand	Red mud Leachate	2:1 Seawater mix	Gypsum addition
pH	13.1	9.7	13.1*
Eh (V)	0.023[#]	0.200	0.023
Selected ions (mg L^{-1})			
Total inorganic carbon	2500[#]	930	2500[#]
Al	352	117.3	352
As	8.1	2.7	8.1
Ca	2	278	48**
Chloride	83[#]	12923	83[#]
K	420	400	420
Mg	0	863	0
Na	701[#]	7401	701[#]
Sulphate	2010	2470	2010
V	15.6	5.2	15.6

*modelled at the point of first addition
**Based on Ksp for gypsum of $10^{-4.60}$
[#] Data from [23].

Table S3. Mineral saturation indexes based on the red mud leachate, gypsum amended leachate and 2:1 seawater mix compositions given in (SI Table S1). Results based on PHREEQC modelling. Major phases calculated using data from pitzer.dat* / minteq.dat, MINTEQ (V phases), Bothe and Brown, [24] (additional Ca-arsenate hydrate phases).

Saturation Index		**Red mud**	**Gypsum**	***Sea water mix**
Phase	**Species**			
$Al(OH)_3(a)$	$Al(OH)_3$	-1.81	-1.79	**1.04**
Alunite	$KAl3(SO_4)2(OH)_6$	**27.74**	**3.75**	-64.88
Aragonite	$CaCO_3$	**0.18**	**2.13**	**1.89**
Boehmite	AlOOH	-0.05	-0.03	**2.81**
Brucite	$Mg(OH)_2$	-	-0.71	0.33
Calcite	$CaCO_3$	**0.24**	**2.33**	**2.06**
Diaspore	AlOOH	**1.79**	**1.81**	**4.65**
Gibbsite	$Al(OH)_3$	**13.68**	**-0.01**	**2.82**
Gypsum	$CaSO_4.2H_2O$	-2.50	-0.59	-43.35
Halite	NaCl	-5.92	-5.87	-2.80
Magnesite	$MgCO_3$	-	**0.56**	**2.15**
As phases				
$AlAsO_4{:}H_2O$	$AlAsO_4{:}H_2O$	-18.36	-18.48	-7.74
Arsenolite	As_4O_6	-115.07	-115.62	-56.75
As_2O_5	As_2O_5	-53.27	-53.54	-37.72
Claudetite	As_4O_6	-114.84	-115.39	-56.53
$Ca_3(AsO_4).4¼H_2O$	$Ca_3(AsO_4).4¼H_2O$	-4.97	-0.58	-3.12
$Ca_3(AsO_4).3⅜H_2O$	$Ca_3(AsO_4).3⅜H_2O$	-45.13	-40.73	-43.26
$Ca_4(OH)_2(AsO_4)_2.4H_2O$	$Ca_4(OH)_2(AsO_4)_2.4H_2O$	-61.13	-55.18	-63.83
$Ca_5(AsO_4)_3OH$	$Ca_5(AsO_4)_3OH$	-78.13	-70.76	-77.59
$CaHAsO_4.H_2O$	$CaHAsO_4.H_2O$	-27.47	-26.05	-24.26
Ferrarisite	$Ca_5H_2(AsO_4)_4.9H_2O$	-100.99	-93.75	-92.71
Guerinite	$Ca_5H_2(AsO_4)_4.9H_2O$	-100.19	-92.95	-91.91
V phases				
$Ca_2V_2O_7$	$Ca_2V_2O_7$	-3.11	-1.44	-1.96
$Ca_3(VO_4)_2$	$Ca_3(VO_4)_2$	-3.85	-1.40	-4.98
Ca-vanadate	$Ca_{0.5}VO_3$	-7.46	-6.57	-4.03
$Mg_2V_2O_7$	$Mg_2V_2O_7$	-	-	-6.42
Na_3VO_4	Na_3VO_4	-19.11	-18.91	-20.62
$Na_4V_2O_7$	$Na_4V_2O_7$	-11.55	-11.38	-12.82
Na-vanadate	$NaVO_3$	-7.37	-7.22	-4.07
$V(OH)_3$	$V(OH)_3$	-25.21	-25.10	-12.71
V_2O_3	V_2O_3	-23.23	-23.11	-10.72
V_2O_4	V_2O_4	-15.12	-15.01	-6.01
V_2O_5	V_2O_5	-14.30	-14.18	-8.59
V_3O_5	V_3O_5	-60.73	-60.39	-26.60
V_4O_7	V_4O_7	-76.91	-76.45	-111.0
V_6O_{13}	V_6O_{13}	-79.82	-79.13	-31.97
VCl_2	VCl_2	-82.13	-81.97	-55.16
VCl_3	VCl_3	-88.53	-88.36	-59.44
VMetal	VMetal	-102.91	-102.79	-80.19
VO	VO	-45.25	-45.13	-29.33
$VO(OH)_2$	$VO(OH)_2$	-16.16	-16.04	-7.05

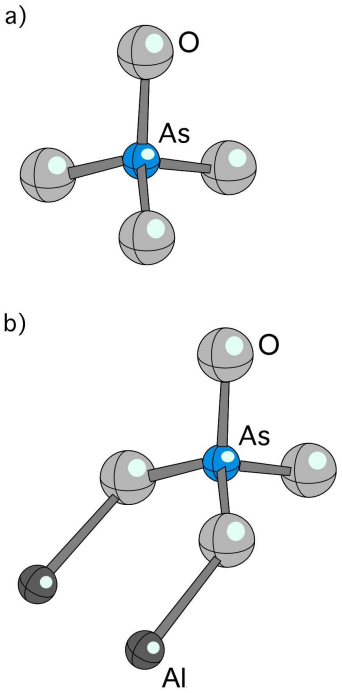

Figure S1. Clusters used to model As EXAFS data of (a) Isolated arsenate tetrahedron; (b) Bidentate arsenate-Al oxyhydroxide surface complex. As = arsenic; O = oxygen; Al = aluminium.

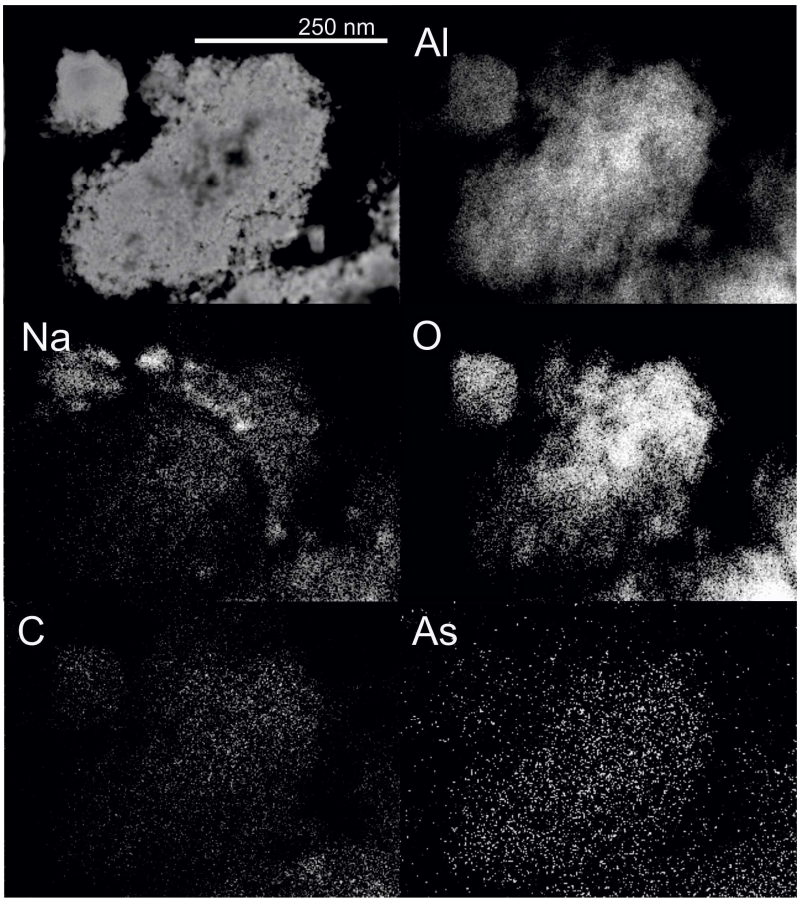

Figure S2. Low resolution dark field (S)TEM image of the precipitate formed by neutralisation of red mud leachate by HCl and selected EDX elemental maps of the same location.

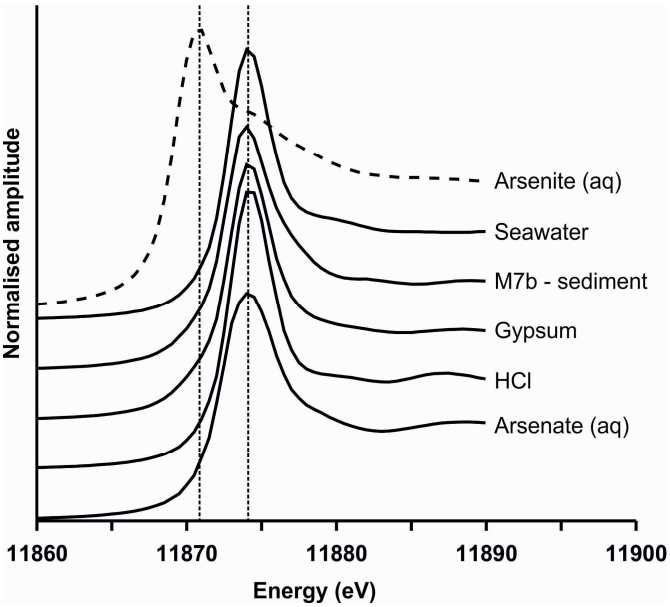

Figure S3. Normalised As K-edge XANES spectra collected from precipitates formed during red mud leachate neutralisation, the M7b river sediment and 1000 mg L^{-1} arsenic standard solutions. Vertical lines are shown to guide the eye.

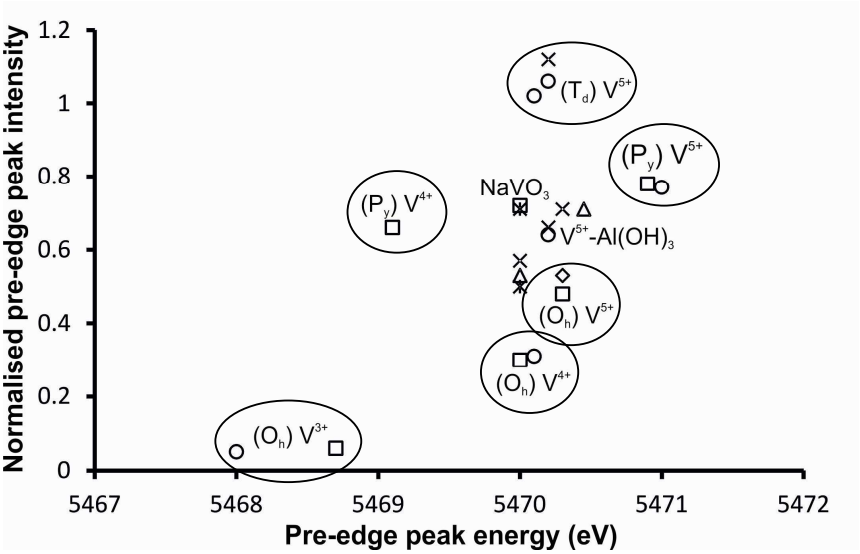

Figure S4. Plot of pre-edge intensity vs. pre-edge peak energy derived from V K-edge XANES spectra. Symbols: (✕) refers to the leachate precipitates and M7b stream sediment and (○) standards from this study; (□) refers to standards taken from [2, 14]; (✳) refers to Ajka red mud samples[17]; (◇) refers to a sample of V^{5+} sorbed to Mg/Al layered double hydroxide [13]; (△) refers to samples of V^{5+} sorbed to oxide surfaces [14, 15]. (T_d), (P_y) and (O_h) refers to tetrahedral, square pyramidal and octahedral co-ordination respectively.

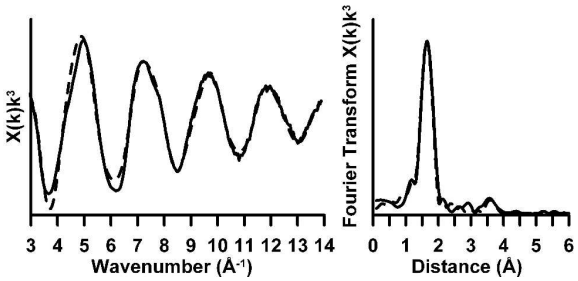

Figure S5. Right: Background subtracted As K-edge EXAFS spectra collected from a precipitated hydrous Ca arsenate. Left: Corresponding Fourier transform calculated from EXAFS spectra. Dashed lines represent a shell by shell DLexcurv V1.0 model fits using the following parameters: 4 O atoms @ 1.69 $\pm$0.02 Å ($2\sigma^2$ (Å^2) = 0.007); 1 Ca atom at 3.67 $\pm$0.05 Å ($2\sigma^2$ (Å^2) = 0.013) (*R* = 15.1; Ef = -14.7). The contribution from multiple scattering pathways were not considered during fitting.

Supporting Information References

1. Ravel, B.; Newville, M.; , ATHENA, ARTEMIS, HEPHAESTUS: data analysis for X-ray absorption spectroscopy using IFEFFIT. *J. Synchrot. Radiat.* **2005**, 537-541.
2. Chaurand, P.; Rose, J.; Briois, V.; Salome, M.; Proux, O.; Nassif, V.; Olivi, L.; Susini, J.; Hazemann, J.-L.; Bottero, J.-Y., New methodological approach for the vanadium K-edge X-ray absorption near-edge structure interpretation: Application to the speciation of vanadium in oxide phases from steel slag. *Journal of Physical Chemistry B* **2007,** *111*, (19), 5101-5110.
3. Tenderholt, A.; Hedman, B.; Hodgson, K. O., PySpline: A modern, cross-platform program for the processing of raw averaged XAS edge and EXAFS data. In *X-Ray Absorption Fine Structure-XAFS13*, Hedman, B.; Painetta, P., Eds. 2007; pp 105-107.
4. Tomic, S.; Searle, B. G.; Wander, A.; Harrison, N. M.; Dent, A. J.; Mosselmans, J. F. W.; Inglesfield, J. E. *New Tools for the Analysis of EXAFS: The DL_EXCURV Package; CCLRC Technical Report DL-TR-2005-001*; Daresbury, UK, 2005.
5. Gurman, S. J.; Binsted, N.; Ross, I., A RAPID, EXACT CURVED-WAVE THEORY FOR EXAFS CALCULATIONS. *Journal of Physics C-Solid State Physics* **1984,** *17*, (1), 143-151.
6. Binsted, N., *CLRC Daresbury Laboratory EXCURV98 program*. CLRC Daresbury Laboratory: Warrington, UK, 1998.
7. Binsted, N.; Strange, R. W.; Hasnain, S. S., CONSTRAINED AND RESTRAINED REFINEMENT IN EXAFS DATA-ANALYSIS WITH CURVED WAVE THEORY. *Biochemistry* **1992,** *31*, (48), 12117-12125.
8. Binsted, N.; Hasnain, S. S., State-of-the-art analysis of whole X-ray absorption spectra. *Journal of Synchrotron Radiation* **1996,** *3*, 185-196.
9. Peacock, C. L., Physiochemical controls on the crystal-chemistry of Ni in birnessite: Genetic implications for ferromanganese precipitates. *Geochimica Et Cosmochimica Acta* **2009,** *73*, (12), 3568-3578.
10. Stern, E. A., Number of relevant independent points in x-ray-absorption fine-structure spectra. *Physical Review B* **1993,** *48*, (13), 9825-9827.
11. Booth, C. H.; Hu, Y. J. In *Confirmation of standard error analysis techniques applied to EXAFS using simulations*, 14th International Conference on X-Ray Absorption Fine Structure, Bristol, UK, 2009; DiCicco, A.; Filipponi, A., Eds. Iop Publishing Ltd: Bristol, UK, 2009.
12. Burke, I. T.; Boothman, C.; Lloyd, J. R.; Mortimer, R. J. G.; Livens, F. R.; Morris, K., Effects of Progressive Anoxia on the Solubility of Technetium in Sediments. *Environmental Science & Technology* **2005,** *39*, (11), 4109-4116.
13. Goh, K. H.; Lim, T. T.; Dong, Z. L., Removal of arsenate from aqueous solution by nanocrystalline Mg/Al layered double hydroxide: sorption characteristics, prospects, and challenges. *Water Sci. Technol.* **2010,** *61*, (6), 1411-1417.
14. Bronkema, J. L.; Bell, A. T., Mechanistic studies of methanol oxidation to formaldehyde on isolated vanadate sites supported on MCM-48. *Journal of Physical Chemistry C* **2007,** *111*, (1), 420-430.
15. Tanaka, T.; Yamashita, H.; Tsuchitani, R.; Funabiki, T.; Yoshida, S., X-ray absorption (EXAFS XANES) study of supported vanadium-oxide catalysts - structure of surface vanadium oxide species on silica and gamma-alumina at a low-level of vanadium loading. *Journal of the Chemical Society-Faraday Transactions I* **1988,** *84*, 2987-2999.
16. Wong, J.; Lytle, F. W.; Messmer, R. P.; Maylotte, D. H., K-edge absorption-spectra of selected vanadium compounds. *Physical Review B* **1984,** *30*, (10), 5596-5610.
17. Burke, I. T.; Mayes, W. M.; Peacock, C. L.; Brown, A. P.; Jarvis, A. P.; Gruiz, K., Speciation of Arsenic, Chromium, and Vanadium in Red Mud Samples from the Ajka Spill Site, Hungary. *Environmental Science & Technology* **2012,** *46*, (6), 3085-3092.
18. Wehrli, B.; Stumm, W., Oxygenation of Vanadyl(IV) - Effect of coordinated surface hydroxyl-groups and OH. *Langmuir* **1988,** *4*, (3), 753-758.
19. Wehrli, B.; Stumm, W., Vanadyl in natural waters - Adsorption and hydrolysis promote oxygenation. *Geochimica et Cosmochimica Acta* **1989,** *53*, (1), 69-77.
20. Wehrli, B.; Sulzberger, B.; Stumm, W., Redox processes catalysed by hydrous oxide surfaces. *Chemical Geology* **1989,** *78*, (3-4), 167-179.
21. Szilagyi, J.; Kovacs, A., A calibration-free evapotranspiration mapping technique for spatially-distributed regional-scale hydrologic modeling. *Journal of Hydrology and Hydromechanics* **2011,** *59*, (2), 118-130.

22. Liu, Y.; Lin, C.; Wu, Y., Characterization of red mud derived from a combined Bayer Process and bauxite calcination method. *Journal of Hazardous Materials* **2007,** *146*, (1-2), 255-261.
23. Mayes, W. M.; Jarvis, A. P.; Burke, I. T.; Walton, M.; Feigl, V.; Klebercz, O.; Gruiz, K., Dispersal and Attenuation of Trace Contaminants Downstream of the Ajka Bauxite Residue (Red Mud) Depository Failure, Hungary. *Environmental Science & Technology* **2011,** *45*, (12), 5147-5155.
24. Bothe Jr, J. V.; Brown, P. W., The stabilities of calcium arsenates at 23Â±1Â°C. *Journal of Hazardous Materials* **1999,** *69*, (2), 197-207.